Formation, evolution, and annihilation of interstitial clusters in ion-implanted Si

Sebania Libertino and Salvatore Coffa
CNR-IMETEM, Stradale Primosole 50, I-95121 Catania, Italy

Janet L. Benton
Bell Laboratories Lucent Technologies, 700 Mountain Avenue, Murray Hill, New Jersey 07974
(Received 20 October 2000; published 20 April 2001)

We review the results of several experiments aimed to elucidate the thermal evolution of the self-interstitial excess introduced by Si-ion implantation in crystalline Si. Deep-level transient spectroscopy and photoluminescence measurements were used to monitor how those interstitials are stored into stable point-like defect structures just after implantation, evolve into defect clusters upon annealing at intermediate temperatures, and are annealed out, releasing the stored self-interstitials upon annealing at larger temperatures. It is shown that although dopant atoms and impurities (C and O) are not the main constituents of these clusters, the impurity content has a large effect on the early stage of cluster formation, at low fluence and low temperatures, and can affect their dissociation kinetics. A stable residual damage, electrically characterized by two signatures at $E_v + 0.33$ eV and $E_v + 0.52$ eV and exhibiting two broad signatures in the photoluminescence spectrum, is present for doses $\geqslant 10^{12}/\mathrm{cm}^2$ and annealing $\geqslant 600$ °C. This residual damage, formed by interstitial clusters, is stable to temperatures as high as 750 °C and anneals out with an activation energy of ~2.3 eV. It is suggested that these clusters store the interstitials that drive transient enhanced diffusion at low implantation doses and/or low temperatures, when no extended defects are formed. Finally, when {311} extended defects form the luminescence spectrum is dominated by a sharp signal at 1376 nm, which we correlate with optical transitions occurring at or close to these defects. Dose and temperature thresholds for the transition from small clusters to extended defects have been observed and will be discussed.

DOI: 10.1103/PhysRevB.63.195206 PACS number(s): 61.72.Cc, 61.72.Ji, 61.72.Tt, 78.55.Ap

I. INTRODUCTION

The supersaturation of Si self-interstitials produced by ion implantation in crystalline Si is responsible of several ion-beam damage related processes such as the formation of extended defects[1] and the transient enhanced diffusion[2] (TED) of dopant atoms. Ion implantation produces interstitial-vacancy (I-V) pairs that are stored into room-temperature stable defect complexes. Moreover, the presence of the extra implanted ion results in an imbalance in the two defect concentrations. Upon annealing, room-temperature stable defect complexes dissociate and the defects (I and V) released undergo extensive recombination in the bulk until only the interstitial excess (due to the extra implanted ions) is left. This process lies at the heart of the so-called ''+1 model,''[3] where it is also assumed that the surface does not play a relevant role during annealing in the first stage. Apart from being quite a crude approximation, the model does not provide any hint on how this interstitial excess is stored in the material. Indeed, due to the high diffusivity and low equilibrium concentration, it is expected that the extra-interstitials will coalesce into more complex defect structures rather than being diluted in the bulk. This behavior has been fully explored for implants at elevated doses. In this case the high I supersaturation produced from the implant ($40\,\mathrm{keV\,Si}$, $5\times10^{13}\,\mathrm{cm}^{-2}$) results, after annealing, in the formation of extended defects such as {311} or dislocation loops that store I and release them when proper thermal budget is provided.[4] The extended defect dissolution maintains an I supersaturation in the material that drives dopant TED in a time scale fixed by their annealing.[5] In particular, the interstitials stored in {311} defects are released with an activation energy of ~3.8 eV, in good agreement with the dopant TED activation energy.[4]

However, recent studies have shown much evidence of TED in samples implanted at low fluence in the early stages of annealing, where extended defects are not formed.[6,7] In particular, ultrafast TED occurs at relatively low temperature (700 °C) and for times from 15 s up to 40 min after low-dose implants (1×10^{11}–$2\times10^{13}\,\mathrm{Si/cm}^2$).[7] The measured activation energy of the process is smaller than that measured during extended defects dissociation, being of the order of 2.3–2.7 eV. It has been proposed that small interstitial clusters, not detectable with transmission electron microscopy[8] (TEM), store the excess interstitials: their dissolution produces the I supersaturation that drives TED.[9] The difficulty to obtain information on the source of the TED in this regime is due to the small dimensions of the agglomerates that store the I supersaturation. While extended defects can be well monitored and characterized by TEM analyses, the structure and the evolution of the nanometer-size I-clusters is undetectable with this technique. Recently, Cowern and co-workers[9] have been able to extract information on the I-cluster dissociation by monitoring its effect on TED. From the measured B TED they extracted the associated I supersaturation. Using inverse modeling of the supersaturation, they found that the growth of small interstitial clusters can be described in terms of a rate-limited transition between two groups of cluster sizes (with a boundary at dimensions of ~10 interstitials). In the fitting procedure they assume that the I-clusters grow through an Ostwald ripening process[10] (OR) and explain the rate-limited transition in terms of the

large variation in the binding energy of last added interstitials in small clusters. However, no direct information on the cluster status and evolution was achieved.

In spite of several investigations of defect evolution, an intriguing question remains unanswered. It is not known if the structural unit of the defect remains unchanged during the growth from small *I*-clusters to {311} defects, or if significant modification in the spatial distribution and binding energy of the *I* to the defect structure occurs. This last scenario is supported by the results of quantum-mechanical calculations. Tight-binding calculations of *I* agglomeration[11] revealed that structures of an *I*-cluster alternative to the {311} defect structure may exist when few interstitials agglomerate. The formation energy per *I* is lower than that necessary for the formation of the (110) chain, which is the building block of the {311} defect, when the number of interstitials is lower than 10. This suggests that small *I*-clusters may not be the direct precursors of the {311} defects and that a structural transformation should occur at some stage of the growth process to allow the extended defect formation.

The aim of this review is to assess the formation of stable damage, able to survive annealing at temperatures above 600 °C where dopant diffusion and formation of secondary defects occur. It is particularly important to establish the structure and electrical behavior of this damage, its ability to store and release point defects that can then interact among themselves or with dopant atoms. Moreover, an extensive study of the *I*-clusters in a region where extended defects are not formed could provide a link between the point-like defects generated by the ion beam and the extended defects, as proposed by Tan.[12]

In the last few years we performed a set of experiments in order to provide information on the structure and evolution of *I*-clusters. We observed experimentally, by using deep-level transient spectroscopy (DLTS) measurements,[13] that *I*-*V* recombination during both implantation and annealing occurs preferentially in the bulk, leaving an excess of *I*-type defects due to the presence of the extra implanted ion.[14,15] These results provide a confirmation of the +1 model in the low-dose regime. Moreover, we have recently established that *I*-clusters introduce deep levels in the band gap that can be monitored by DLTS.[16,17] In this work, we review our latest results and present new data using both DLTS and photoluminescence (PL),[18] on the formation and dissolution kinetics of *I*-clusters and the transition to {311} defects. To this purpose we studied the structure of defect clusters: the ion fluence and annealing temperature regime in which they form are stable and anneal out. Furthermore, the impurity role (C and O) on defect formation and dissociation was assessed and the dissociation energy value for small clusters determined. The results are linked to TED activation energy for low-dose implants ($\leqslant 1\times10^{13}\,\mathrm{cm}^{-2}$) with no extended defect formation. Finally, PL measurements were extensively used to monitor the transition from *I*-clusters to extended defects.

II. EXPERIMENT

Epitaxial (epi with O and C content $[O]\sim[C]\leqslant10^{15}\,\mathrm{cm}^{-3}$ and a resistivity of $\sim2\ \Omega\,\mathrm{cm}$) and Czochralski (CZ, $[O]=7\times10^{17}\,\mathrm{cm}^{-3}$ and $[C]\leqslant10^{16}\,\mathrm{cm}^{-3}$ with a resistivity of 1–4 $\Omega\,\mathrm{cm}$, or with $[O]=1\times10^{18}\,\mathrm{cm}^{-3}$, $[C]\sim10^{16}\,\mathrm{cm}^{-3}$ and a resistivity of $\sim0.4\ \Omega\,\mathrm{cm}$) Si samples were used. The samples were implanted with either 1.2-MeV or 145-keV Si ions to fluences in the range $1\times10^{9}-5\times10^{13}\,\mathrm{cm}^{-2}$. Annealing was performed under a He flux at temperatures in the range 400–750 °C for times ranging from 10 min to 15 h. After annealing, Schottky barriers on *p*-type Si samples were formed by using room-temperature Ti deposition. Deep-level transient spectroscopy measurements were performed using a Bio-Rad DL8000 apparatus. Depth concentration profiles were obtained by changing the reverse bias from 20 to 3 V and maintaining the difference between reverse and filling biases constant and equal to 3 V. Capture kinetic measurements were performed on a Bio-Rad DL4600 instrument by fixing the reverse bias and filling pulse to 10 and 1 V, respectively, and changing the filling time from 10 ms to 700 ns. PL measurements were performed at 17 K using the 488-nm line of an argon laser at a pump power of 50 mW. Light emitted from the sample was dispersed by a monochromator and detected by a liquid-nitrogen-cooled Ge detector. A standard lock-in technique was used to improve the signal-to-noise ratio.

III. RESULTS AND DISCUSSIONS

A. Evolution from point defects to clusters

The defect evolution from point-like structures into *I*-clusters and eventually into extended defects was followed for Si implants in a wide dose range, $1\times10^{9}-5\times10^{13}\,\mathrm{cm}^{-2}$ and upon annealing at temperatures of 400–750 °C. The residual damage left after annealing was monitored and characterized using both electrical (DLTS) and optical (PL) measurements.

The residual damage left after low-dose implantation and annealing at temperatures below 600 °C is mainly formed by point-like secondary defects. The DLTS spectra of *p*-type epitaxial Si samples annealed at 400 °C for 30 min are compared in Fig. 1 for 1.2 MeV Si implantation to doses of $1\times10^{9}\,\mathrm{Si/cm}^2$ (dashed line), $1\times10^{11}\,\mathrm{Si/cm}^2$ (solid line), and $1\times10^{12}\ \mathrm{Si/cm}^2$ (dot-dashed line). The samples were annealed together in the furnace, and the reference sample (unimplanted, not shown) that underwent the same thermal treatment does not exhibit trap levels in concentration above $1\times10^{11}\ \mathrm{traps/cm}^3$ (DLTS sensitivity limit for these samples). The spectra shown in figure clearly show the presence of two different regimes in the residual damage features. The residual damage in samples implanted at low dose, up to $10^{11}\,\mathrm{cm}^{-2}$, is roughly given by the levels identified as H_1 at $E_v+0.08\,\mathrm{eV}$, H_2 at $E_v+0.13\,\mathrm{eV}$, H_3 at $E_v+0.23\,\mathrm{eV}$, H_4 at $E_v+0.25\,\mathrm{eV}$, H_5 at $E_v+0.39\,\mathrm{eV}$, and H_6 at $E_v+0.53\,\mathrm{eV}$, where E_v indicates the top of the valence band. For low doses ($<10^{12}\,\mathrm{cm}^{-2}$) the same signatures within the experimental error (below ±0.01 eV) are observed. An increase in the ion implantation dose in this regime only produces a linear increase in the defect concentration (as will be shown in Fig. 3). These results suggest that at low implantation doses the collision cascades generated by

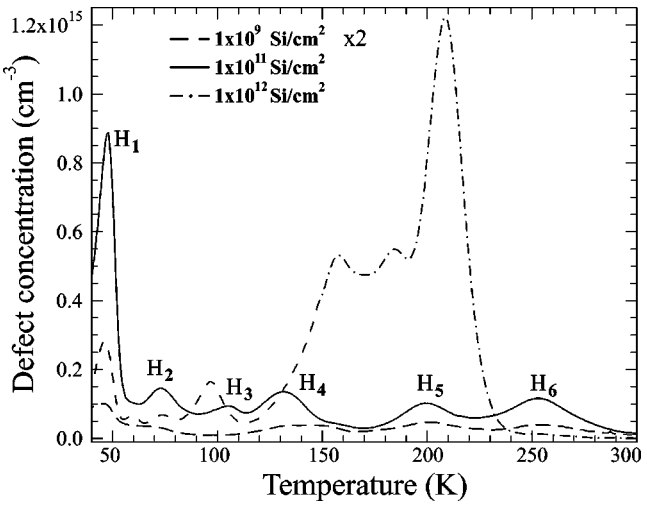

FIG. 1. DLTS spectra measured on *p*-type epitaxial Si implanted with 1.2-MeV Si to a dose of $1\times10^{9}\,\mathrm{cm}^{-2}$ (dashed line), $1\times10^{11}\,\mathrm{cm}^{-2}$ (solid line), and $1\times10^{12}\,\mathrm{cm}^{-2}$ (dot-dashed line). The samples were annealed at 400 °C for 30 min.

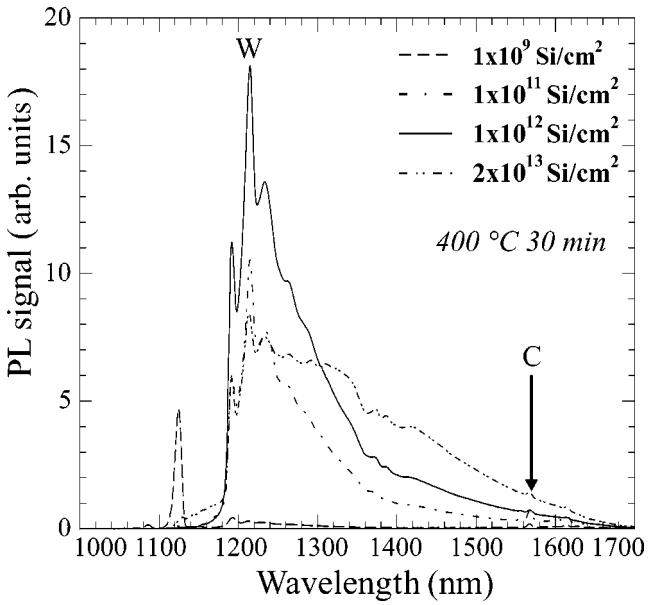

FIG. 2. PL spectra of CZ Si samples implanted with 1.2-MeV Si to doses of $1\times10^{9}\,\mathrm{cm}^{-2}$ (dashed line), $1\times10^{11}\,\mathrm{cm}^{-2}$ (dot-dashed line), $1\times10^{12}\,\mathrm{cm}^{-2}$ (solid line), and $2\times10^{13}\,\mathrm{cm}^{-2}$ (double dot-dashed line). The samples were annealed at 400 °C 30 min.

different ions do not overlap considerably: the final damage configuration depends only on the defect density and the defect interactions within the single ion track. This would explain why the same class of defects is observed regardless of the dose. This hypothesis is confirmed by the evidence that the DLTS signatures at these doses ($\leqslant1\times10^{11}\,\mathrm{cm}^{-2}$) change only as a function of the annealing temperature in the range 400–600 °C.

The other regime observed in Fig. 1 occurs at intermediate dose ($1\times10^{12}\,\mathrm{cm}^{-2}$–$1\times10^{13}\,\mathrm{cm}^{-2}$). The residual damage exhibits characteristics totally different from those previously observed. The DLTS peaks in the high-temperature part of the spectrum, H_3–H_6 are either not present (e.g., H_6) or totally overwhelmed by new defect signatures. Also the DLTS signatures in the low-temperature part of the spectrum (H_1 and H_2) that increase for doses up to 1×10^{11} Si/cm^2 decrease for higher doses. These results suggest that at these high doses a strong interaction between defects of subsequent collision cascades occurs, producing dramatic changes in the residual damage features.

The residual damage features were also monitored by PL measurements on samples, implanted to doses in the range 1×10^{9}–$2\times10^{13}\,\mathrm{cm}^{-2}$ and annealed at 400 °C for 30 min. PL is sensitive to optically active centers, on which the electron-hole recombination occurs, producing photons. To reduce as much as possible the nonradiative recombination paths, all the measurements were carried out at 17 K. Although there are examples in the literature where DLTS and PL have been used to identify the same defect complex, it should be noted that they monitor different centers and it is not always possible to directly link the two techniques. The PL spectra of CZ Si samples implanted with 1.2 MeV Si are compared in Fig. 2. After 1×10^{9} cm^{-2} Si implantation (dashed line) the optically active damage is barely visible, although the phonon-assisted Si band-to-band carrier recombination is clearly visible at 1121 nm (Si band edge). Also other features more evident for higher doses are detected in this sample. After implantation to 10^{11} Si/cm^2 (dot-dashed line), the Si band edge is no longer visible, confirming the results already obtained by DLTS: The damage is present in higher concentration. In this sample most of the radiative recombination occurs at the damage. Identification of the PL lines shows that they belong to *I*-type defects. The *W* line[18] at 1218 nm (1018 eV) is the dominant center for doses $\geqslant1\times10^{11}\,\mathrm{cm}^{-2}$. This line has been recently associated with small *I*-rich clusters.[18,19] Moreover, the shoulder observed at 1279 nm (0.969 eV), is probably the *G* line, associated with a complex between an interstitial and a substitutional C atom (C_iC_s).[18] The spectra also exhibit a peak at 1570 nm (0.789 eV) that can be associated with carbon interstitial oxygen complexes (C_iO_i, the well known *C* line).[18] It should be mentioned that the PL is not quantitative; hence is not possible to extract information on the defect concentration from their PL lines. An increase in the PL signal of these lines is observed for 1×10^{12} Si/cm^2 implantation dose (solid line). PL can be really useful to monitor samples having a high damage concentration, where the DLTS cannot be used due to the large electrical compensation produced by the damage. In fact, it is possible to monitor the residual damage after 2×10^{13} Si/cm^2 implant (double-dot-dashed line). In this case the *W* line is the dominant feature of the spectrum, but a pronounced shoulder between 1300 and 1400 nm appear, probably due to the high degree of disorder in the lattice.

The damage evolution was followed as a function of both the implantation dose and the annealing temperature using DLTS and PL. Between the two techniques, only the DLTS is able to provide quantitative information on the defect concentration. In fact, assuming that every complex involves a single point defect, we added the defect concentration obtained from the DLTS peaks of various spectra (some of which are plotted in Fig. 1) using the procedure reported

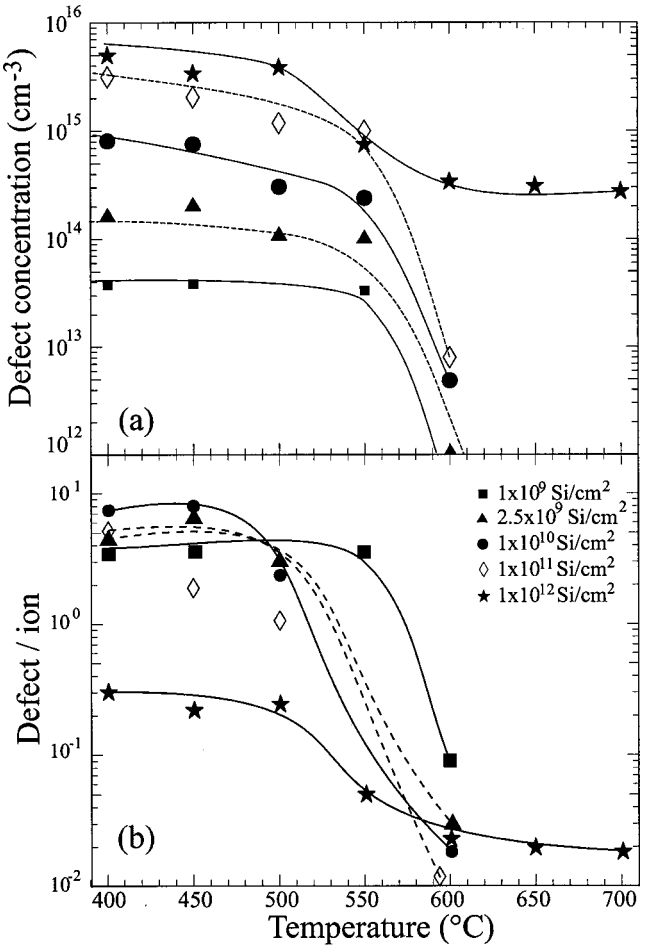

FIG. 3. (a) Total defect concentration and (b) number of defect per ion as a function of isochronal (30-min) annealing at different temperatures. Data were obtained by DLTS measurements, for *p*-type epitaxial Si samples implanted with 1.2 MeV Si to doses of $1\times10^{9}\,\mathrm{cm}^{-2}$ (■), $2.5\times10^{9}\,\mathrm{cm}^{-2}$ (▲), $1\times10^{10}\,\mathrm{cm}^{-2}$ (●), $1\times10^{11}\,\mathrm{cm}^{-2}$ (◇), and $1\times10^{12}\,\mathrm{cm}^{-2}$ (★).

elsewhere.[14,15] The results obtained for 1.2 MeV Si implantation at room temperature on epitaxial Si samples are summarized in Fig. 3. In this figure, the total defect concentration [Fig. 3(a)] and the number of defects per ion [Fig. 3(b), obtained dividing the defect concentration by the ion dose] are plotted as a function of the annealing temperature for isochronal (30 min) annealing in samples implanted to $1\times10^{9}\,\mathrm{cm}^{-2}$ (■), $2.5\times10^{9}\,\mathrm{cm}^{-2}$ (▲), $1\times10^{10}\,\mathrm{cm}^{-2}$ (●), $1\times10^{11}\,\mathrm{cm}^{-2}$ (◇), and $1\times10^{12}\,\mathrm{cm}^{-2}$ (★). The solid and dashed lines are used as a guide to the eye. An increase in the ion dose up to $1\times10^{11}\,\mathrm{cm}^{-2}$ produces a roughly linear increase in the total defect concentration as previously mentioned (see Fig. 1). In fact, the sum of the defect signatures measured by DLTS, H_1-H_6, for the dose range $1\times10^{9}-1\times10^{11}\,\mathrm{cm}^{-2}$ after 400 °C annealing at 30 min, shows a linear increase. However, increasing the temperature at 600 °C, a dramatic reduction of the defect concentration is produced, suggesting that the implantation damage is fully recovered. The lattice recovery for annealing at 600 °C in samples implanted to doses up to $10^{11}\,\mathrm{cm}^{-2}$ is confirmed by the PL

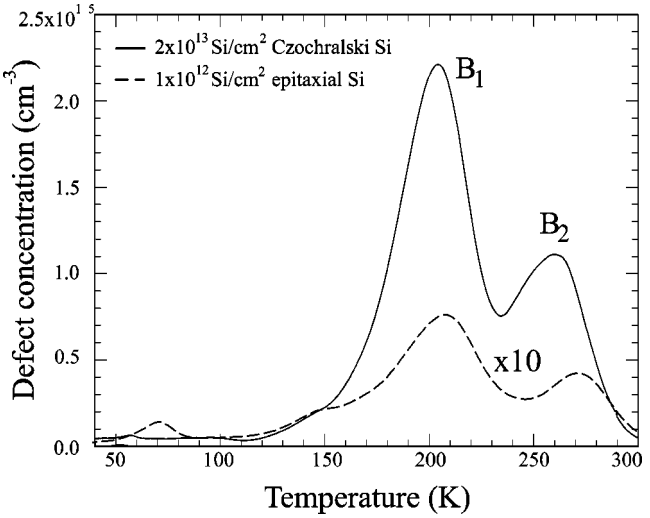

FIG. 4. DLTS spectra measured on *p*-type CZ Si implanted with 145-keV Si to a dose of $2\times10^{13}\,\mathrm{cm}^{-2}$ and annealed at 680 °C for 1 h (solid line) and on *p*-type epitaxial Si implanted with 1.2 MeV Si to a dose of $1\times10^{12}\,\mathrm{cm}^{-2}$ and annealed at 600 °C for 30 min (dashed line, multiplied by a factor of 10).

measurements that only exhibit the band-edge recombination line for those samples (not shown).

The data for ion implantation to larger doses ($\geqslant1\times10^{12}\,\mathrm{Si/cm}^2$) reveal a quite different behavior. First, the DLTS spectra of samples annealed at temperatures $\leqslant500$ °C exhibit a residual damage dramatically different from that observed in samples implanted to lower doses (see Fig. 1). Furthermore, the damage is still detectable in DLTS after annealing at temperatures $\geqslant600$ °C, as shown in Fig. 3. These results strongly suggest that a more stable class of defects is formed at this dose. We believe that this difference arises from the higher interstitial supersaturation obtained for higher dose implants. This, in fact, allows the formation of more complex defects already in the early stages of annealing.

Another effect of the modification in the defect structure is visible in Fig. 3(b), where the number of defects per ion is plotted according to the counting[14,15] procedure. Once again, for doses up to $10^{11}\,\mathrm{cm}^{-2}$ the defect concentration increases roughly linearly [see Fig. 3(a)]; hence the number of defects per ion remains roughly constant at ~3 regardless of the dose. For implants at $1\times10^{12}\,\mathrm{Si/cm}^2$ the number of defects per ion obtained with the same method is much lower, suggesting that the simple counting procedure used for lower doses cannot be applied.

B. Characterization of Si interstitial clusters

The defects formed after implants at doses of $1\times10^{12}\,\mathrm{Si/cm}^2$ or higher are very stable in temperature and are still present after 750 °C, 30 min annealing. It is therefore interesting to characterize the residual damage obtained in this dose regime in more details.

1. Electrical and optical properties

The DLTS analysis of samples implanted at doses $\geqslant10^{12}\,\mathrm{cm}^{-2}$ and annealed in a wide range of temperatures

and times show (see Fig. 4) that the same class of defects is formed regardless of the annealing conditions. In particular, in Fig. 4 the DLTS spectrum of a sample implanted with 145 keV Si to a dose of $2\times10^{13}\,\mathrm{cm}^{-2}$ on *p*-type Czochralski-grown Si and annealed at 680 °C, 1 h (solid line) is compared with a sample implanted with 1.2 MeV Si to a dose of $1\times10^{12}\,\mathrm{cm}^{-2}$ on *p*-type epitaxial Si and annealed at 600 °C, 30 min (dashed line). It should be noted that this last spectrum has been multiplied by a factor of 10 to allow comparison. The residual damage for the two samples is mainly given by two distinct signatures having activation energies of $E_v+0.33\,\mathrm{eV}$ and $E_v+0.52\,\mathrm{eV}$ and labeled in Fig. 4 as B_1 and B_2 (*B*-lines), respectively.[15,20] Similar defect signatures have been detected regardless of the ion-implantation energy, dose, and impurity content of the sample. The O and C contents are, respectively, 3 and 1 order of magnitude higher in CZ ($\sim1\times10^{18}\,\mathrm{O/cm^3}$, $\sim1\times10^{16}$ C/cm^3) than in epi Si ($[\mathrm{O}]\sim[\mathrm{C}]\sim1\times10^{15}\,\mathrm{cm}^{-3}$). Also the dopant concentration does not affect the damage signal, since the CZ Si wafers used have about one order of magnitude more B than the epi Si. Moreover, in contrast to the low-dose ($<10^{11}\,\mathrm{Si/cm^2}$) residual damage, the thermal treatment is not the dominant factor in determining the final defect characteristics.

These results and more extensive studies[16,17] confirm that neither the impurities, O or C, nor the dopant, B, are the main constituents of these defects. The same defect signatures are observed regardless of the implantation dose for doses $\geqslant1\times10^{12}\,\mathrm{Si/cm^2}$. It should be mentioned that DLTS measurements exhibit small differences, within ±0.05 eV ($\sim$10%), in the activation energy values for the two lines (B_1 and B_2), but they have not been successfully correlated with any difference in the sample characteristics, implantation conditions, or thermal treatment. Moreover, since the residual damage features after high-dose implantation do not depend on the impurity concentration for wide dose, temperature, and time ranges, it is confirmed that they are particularly stable defect structures, probably clusters of intrinsic defects.

The PL spectra of *p*-type (solid line) and *n*-type (dashed line) CZ Si samples implanted with 1.2 MeV Si to a fluence of $1\times10^{13}\,\mathrm{cm}^{-2}$ and annealed at 600 °C for 30 min are compared in Fig. 5. The same optically active centers are observed in both *n*- and *p*-type Si under the same laser pumping power (50 mW) and temperature (17 K) conditions. The optically active residual damage is the same regardless of the dopant (P and B, respectively). This result shows that the dopant (P or B) does not influence the residual damage features, as previously observed for the electrically active residual damage.

The PL spectra present two main features in the 1100–1400 nm range, consisting of two broad peaks centered at 1320 nm (0.94 eV) and 1390 nm (0.89 eV). These two features are broad luminescence bands and do not arise from the convolution of narrower peaks.[21] The broadening in the PL peak has been associated[22] with the quantum confinement of carriers in regions with the high strain surrounding the defects. We will comment further on PL peak broadening later.

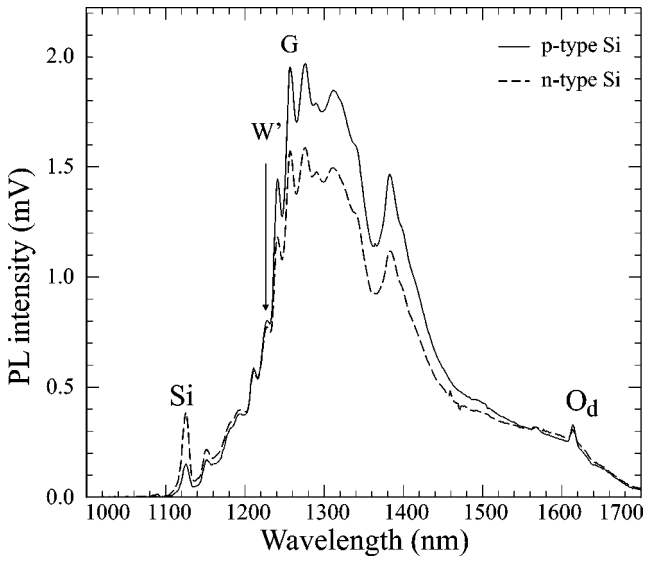

FIG. 5. PL signal for *p*-type (solid line) and *n*-type (dashed line) Si implanted with 1.2 MeV Si to a dose of $1\times10^{13}\,\mathrm{cm}^{-2}$ and annealed at 600 °C for 30 min.

Several sharp lines in the range 1200–1280 nm are superimposed to these broad peaks. All of them have been associated[18] with point-like defect and defect-impurity complexes formed as a consequence of ion-beam irradiation. In particular, a line W' at 1233 nm (1.0048 eV), which is a perturbed form of the *W* line (1218 nm, 1.018 eV), has been identified.[18] As previously mentioned, this line is associated with small *I*-rich clusters.[18,19] The line at 1279 nm (0.969 eV) is the *G* line due to the C_iC_s complex.[18] The spectra also exhibit the well-known *C* line at 1570 nm (0.789 eV) associated with the C_iO_i complexes[18] and two peaks at 1620 nm (0.765 eV) and 1660 nm (0.7466 eV) that can be associated with oxygen thermal donors.[23]

To be sure that after 1.2-MeV Si implantation the signal detected is due only to *I*-type defects or clusters, we measured the PL spectra of samples implanted with 40 keV Si that underwent the same thermal treatments. The same lines are observed, thus ruling out that some of the PL lines observed in Fig. 5 are related to vacancy clusters.

Although the comparison of DLTS and PL measurements does not allow us to conclude that the optically active centers and the electrically active centers belong to the same defect clusters, both data sets can be easily associated with the residual damage, and in both cases, the dopant is not responsible for the final defect characteristics. Both measurements show the presence of a stable class of damage that does not depend on the impurity or dopant concentration or type.

We performed PL measurements in wide dose (1×10^{12}–$1\times10^{14}\,\mathrm{cm}^{-2}$), temperature (550–750 °C), and time (10 min–15 h) ranges and the same optical signatures are always detected, similar to the electrically active defects already shown in Fig. 4. As an example, the PL spectra of *n*-type CZ Si samples implanted with 1.2-MeV Si to doses of $1\times10^{11}\,\mathrm{cm}^{-2}$ (dots), $1\times10^{12}\,\mathrm{cm}^{-2}$ (solid line), $1\times10^{13}\,\mathrm{cm}^{-2}$ (dashed line), and $2\times10^{13}\,\mathrm{cm}^{-2}$ (dot-dashed line), annealed at 600 °C, 30 min, are plotted in Fig. 6. Si ion

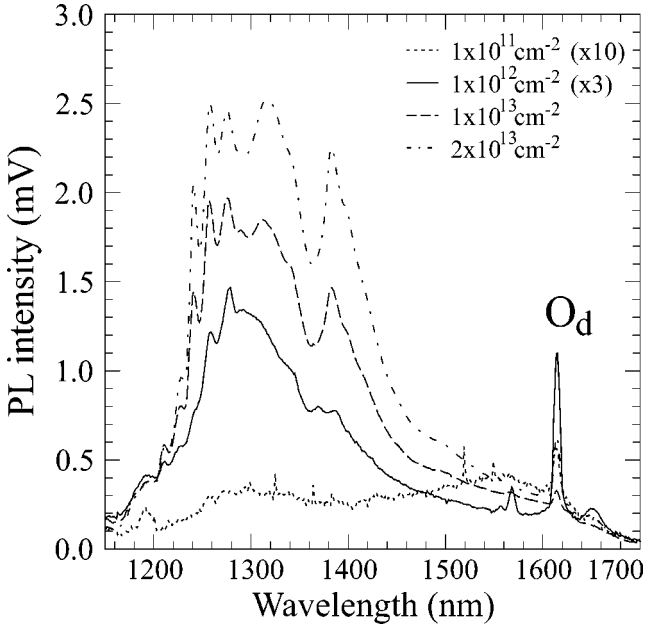

FIG. 6. PL spectra of *n*-type Si implanted with 1.2 MeV Si to doses of $1\times10^{11}\,\mathrm{cm}^{-2}$ (dots multiplied by a factor of 10), $1\times10^{12}\,\mathrm{cm}^{-2}$ (solid line, multiplied by a factor of 3), $1\times10^{13}\,\mathrm{cm}^{-2}$ (dashed line), and $2\times10^{13}\,\mathrm{cm}^{-2}$ (dot-dashed line) annealed at 600 °C for 30 min.

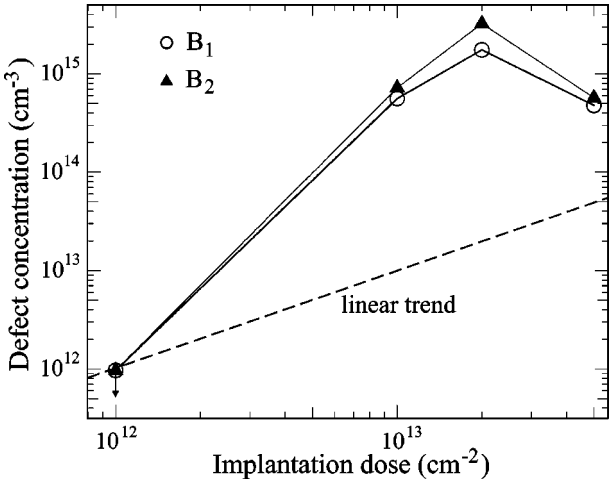

FIG. 7. Defect concentration of B_1 (○) and B_2 (▲) as a function of the implantation dose for *p*-type CZ Si implanted with 145 keV Si after annealing at 680 °C for 1 h. The arrow indicates that the point at $1\times10^{12}\,\mathrm{cm}^{-2}$ is an upper value due to the DLTS sensitivity limit. The dashed line shows a linear trend.

implantation at low doses does not cause the formation of optically active centers after annealing, as the PL spectrum (multiplied in the figure by a factor of 10) of the sample implanted at $1\times10^{11}\,\mathrm{Si/cm}^2$ confirms. For higher doses, $\geqslant10^{12}\,\mathrm{cm}^{-2}$, the intensity of the spectra increases with ion dose but the major features remain unchanged. All the spectra exhibit the oxygen thermal donor peak (O_d) at 1620 nm, already observed in Fig. 5. Note that the intensity of these lines is reduced when the dose is increased. It suggests that the centers responsible for these features compete with those responsible of the 1200–1400 nm features in trapping recombining excess carriers. Finally, TEM analyses revealed that no extended defects are formed in these samples even after at $2\times10^{13}\,\mathrm{cm}^{-2}$ Si ion implantation.[21]

The two features at 1320 nm (0.94 eV) and 1390 nm (0.89 eV) are unchanged as a function of the ion-implantation dose. Broad features in PL spectra have been usually observed[22] in samples having extended defects, such as in oxygen-precipitated, antimony-precipitated, and hydrogen-plasma-treated silicon. The broadening has been associated with the quantum confinement of carriers in regions with the high strain surrounding the defects. Since no extended defects are detected in our samples, we believe that these signatures are associated with carrier recombination in the strained region surrounding the small *I*-clusters embedded in the Si matrix.[21] In the next section (Sec. III C) it will be shown that the cluster electrical signatures (*B*-lines) also exhibit a broadening that could be associated with the same cause: the strain introduced by the defects.

These PL results suggest that the material contains *I*-rich regions where *I*-type point-defect complexes (such as C_iO_i and C_iC_s), small *I*-complexes (the *W* line), and larger *I*-clusters are present. Since we did not observe any *V*-type defect signatures, we believe that the *I* excess observed is the direct consequence of the extra implanted ion, introduced during implantation.

Since PL measurements are not quantitative, to get information on defect concentrations and introduction rates, DLTS measurements were used. The defect concentration as a function of the ion-implantation dose from 1×10^{12} to $5\times10^{13}\,\mathrm{cm}^{-2}$ for 145 keV Si implants for both defects B_1 (○) and B_2 (▲) after annealing at 680 °C for 1 h is plotted in Fig. 7. The annealing temperature, 680 °C, allows the formation of extended defects at the highest dose, as will be shown in Sec. III D. The comparison with a linear trend, the dashed line in the figure, clearly shows that the defect formation rate is strongly nonlinear as the implantation dose is increased. For $1\times10^{12}\,\mathrm{Si/cm}^2$ implantation, only an upper estimation of the defect concentration is given, as indicated by the arrow, since it is below the sensitivity limit of the DLTS. Finally, the strong reduction in the defect concentration at $5\times10^{13}\,\mathrm{Si/cm}^2$, about one order of magnitude, can be attributed to the formation of extended {311} defects, obtained at fluences above $2\times10^{13}\,\mathrm{cm}^{-2}$, that compete with the *B*-lines in storing the interstitial excess.[15] These results confirm the *I* nature of the clusters, since their concentrations reduce when *I*-type extended defects form.

Another evidence of the complex nature of these defects is provided by their depth-concentration profiles, as determined by DLTS. The depth-concentration profile of a point-like interstitial defect, the C_iO_i (●), and of B_1 (■) are shown in Figs. 8(a) and 8(b), respectively, and are compared with the Frenkel-pair (dashed line) and the extra ion (solid line) distributions simulated by MARLOWE,[24] a Monte Carlo code. The experimental profile of the C_iO_i (obtained after 1.2 MeV Si ion implantation to a fluence of $1\times10^{9}\,\mathrm{cm}^{-2}$) precisely mirrors the simulated Frenkel-pair profile. The extra ion profile simulation shows a narrower and slightly deeper peak. On the other hand, the B_1 depth profile, obtained after 1.2

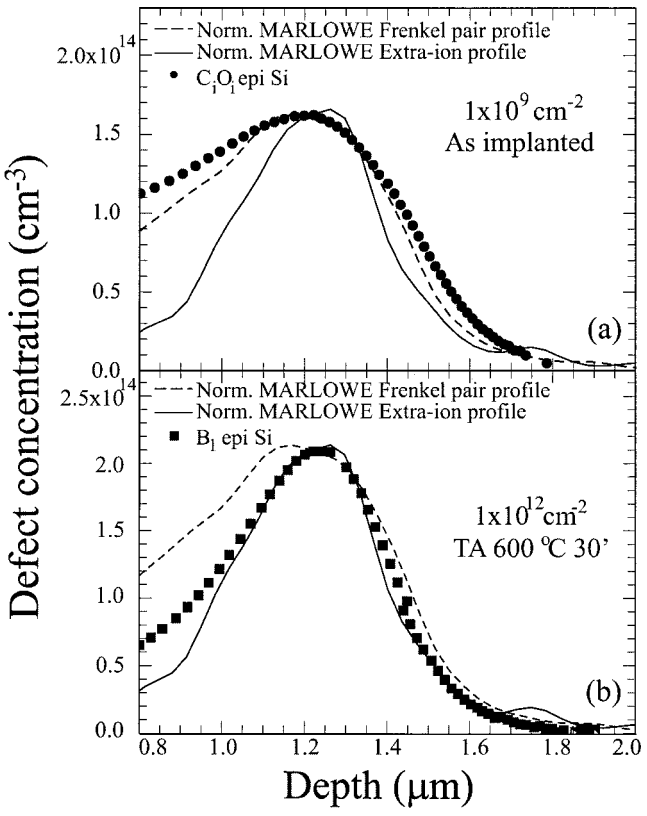

FIG. 8. Depth-concentration profile of (a) C_iO_i defect pairs (●) in a *p*-type epitaxial Si sample implanted with 1.2 MeV Si to a dose of $1\times10^9\,\mathrm{cm}^{-2}$, (b) B_1 line (■) in a *p*-type epitaxial Si sample implanted with 1.2-MeV Si to a dose of $1\times10^{12}\,\mathrm{cm}^{-2}$ and annealed at 600 °C for 30 min. The lines are a depth profile simulation of the implanted ion (solid line) and of the of Frenkel pairs generated by the beam (dashed line).

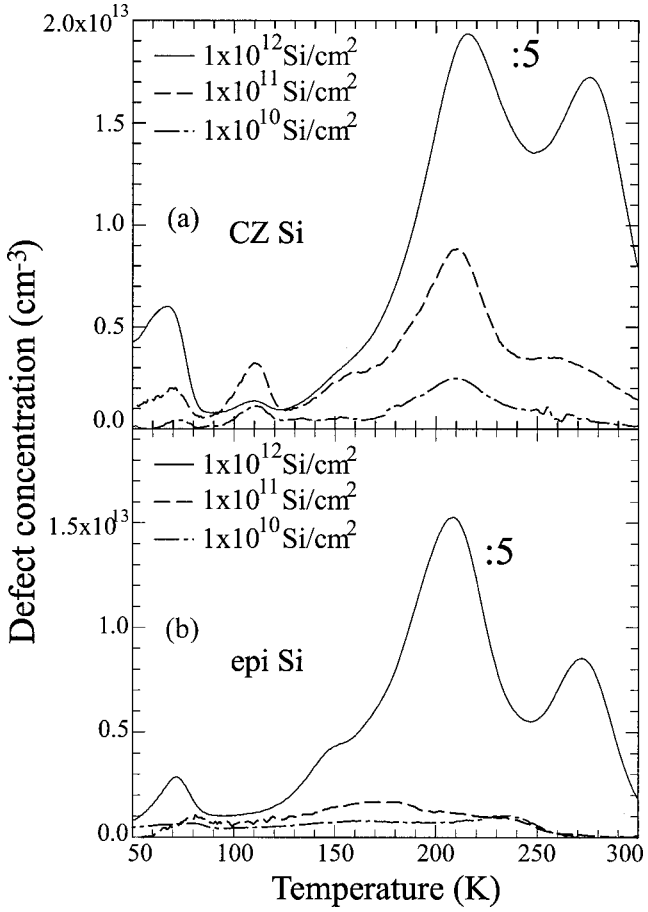

FIG. 9. DLTS spectra measured on *p*-type (a) CZ and (b) epitaxial Si samples implanted with 1.2 MeV Si to doses of $1\times10^{10}\,\mathrm{cm}^{-2}$ (dot-dashed lines), $1\times10^{11}\,\mathrm{cm}^{-2}$ (dashed lines), and $1\times10^{12}\,\mathrm{cm}^{-2}$ (solid lines, divided by a factor of 5). All samples were annealed at 600 °C for 30 min.

MeV Si ion implantation to a fluence of $1\times10^{12}\,\mathrm{cm}^{-2}$ and annealing at 600 °C for 30 min, exhibits a maximum at ~1.3 μm and precisely mirrors the simulation profile of the extra implanted ion at this dose (divided by a factor 100 to allow comparison). Similar depth profiles have been measured for B_2 (not shown). These considerations and the result that the *B*-lines defect structures form in the end of range region, which is the region that experiences the maximum supersaturation of interstitials, support the conclusion that these defects are Si interstitial clusters.

2. Early stages of interstitial cluster formation

The next issue to be addressed is the formation kinetics of the interstitial clusters. In particular, the existence of a threshold dose for their formation and its dependence on the impurity content are of great interest. In this section, it is shown that the presence of impurities (O and C) in the Si sample modifies the kinetics of defect formation and dissolution, although the cluster defects do not contain large numbers of C or O. We monitored the residual damage as a function of the implantation dose and of the material impurity concentration and the results are summarized in Fig. 9. The DLTS spectra for both Czochralski [Fig. 9(a)] and epi [Fig. 9(b)] *p*-type Si samples implanted with 1.2 MeV Si to fluences of $1\times10^{10}\,\mathrm{cm}^{-2}$ (dot dashed line), $1\times10^{11}\,\mathrm{cm}^{-2}$ (dashed line), and $1\times10^{12}\,\mathrm{cm}^{-2}$ (solid line, both spectra have been divided by a factor of 5 to allow comparison) are plotted in figure. All samples underwent annealing at 600 °C for 30 min. The DLTS spectra on epi Si show that the defect concentration is $\leqslant2\times10^{12}\,\mathrm{cm}^{-3}$ for doses below $1\times10^{12}\,\mathrm{Si/cm}^2$ while CZ Si samples show the B_1 signature after implants to $1\times10^{10}\,\mathrm{Si/cm}^2$ and the cluster signatures are already visible[17] at $10^{11}\,\mathrm{Si/cm}^2$, even if their concentration is quite low ($<1\times10^{13}\,\mathrm{cm}^{-3}$). The figure clearly shows that at least one of the *B*-lines is formed at lower doses in CZ Si, which has a higher impurity content.

The comparison of these results with those shown in the previous subsection indicates that the impurity presence plays a role in the *I*-cluster formation only for low doses ($\leqslant10^{11}\,\mathrm{cm}^{-2}$) Si ion implantation. The experimental data are explained assuming that only clusters above certain dimension can survive annealing at 600 °C for 30 min. As a result, very small clusters, e.g., formed by Si implantation of $1\times10^{11}\,\mathrm{cm}^{-2}$, tend to dissociate at times much shorter than 30 min. This is what is observed in epi Si, where the *I* generated by the implant can be stored only in small clusters. A different scenario is proposed for the CZ Si case where the

impurity presence favors I trapping. In fact, it is known that impurities, in particular, C, are efficient traps for I,[25,26] storing them in small defects, thus preventing the formation of a bigger cluster[27] or extended defects. C and I might form mobile C-I complexes[28] followed by the nucleation and growth of C-I agglomerates.[29] The impurities reduce the Si I diffusion length by trapping and releasing them, preventing their annealing to the surface and causing a local high supersaturation in the end of range region. As a result the cluster structures rapidly grow above the critical size to be stable. This effect is visible only at low doses. In fact, as the implantation dose exceeds a critical value, which we estimated to be 1×10^{12} Si/cm^2, the I supersaturation allows the fast growth of I-clusters. Our interpretation of the data is confirmed by the evidence that extended defects are known[25,26] to form at a threshold dose that increases with the sample impurity content. Moreover, it will be shown that the thermal stability of clusters strongly depends on the implantation dose.[17,30]

3. Dissolution of interstitial clusters

In order to verify if the interstitials stored into small I-clusters might be responsible for TED phenomena at low implantation dose, we studied the I-cluster annealing behavior. In particular, we studied the dissociation energy by measuring the residual damage as a function of the annealing time and temperature by DLTS. The analysis of the DLTS spectra at different annealing times for a given temperature gives the characteristic annealing time τ_0 at that temperature. These values were determined by fitting the data obtained for annealing at temperatures ranging from 550 °C (30 min–15 h) to 700 °C (10–40 min) for epitaxial Si implanted with 1.2 MeV Si to a fluence of 1×10^{12} cm^{-2}. The characteristic time (τ_0) is given by the relation

$$C(t)=C_0\exp\left(-\frac{t}{\tau_0}\right), \tag{1}$$

where C_0 is the initial cluster concentration. The concentration values used for determination of τ_0 have been determined from the data according with the procedure explained in the next section.

The τ_0 values at the temperatures explored are summarized in the Arrhenius plot shown in Fig. 10 for both B_1 (□) and B_2 (○). The best fits of the data are plotted in the figure as a solid and dashed line for B_1 and B_2, respectively. The slope of the fits provides an estimation of the activation energy for dissociation. In particular, dissociation energy values of 2.28 and 2.36 eV are obtained for B_1 and B_2, respectively. These values, equal within the experimental errors (~15%), are consistent with the TED characteristic energy in absence of extended defects.[6–9]

In addition, we monitored the B-line dissociation as a function of the implantation dose. The results for B_2 are summarized in Fig. 11. Similar results have been achieved for B_1 (not shown). The samples were implanted with 145 keV Si to a fluence of 1×10^{12} cm^{-2} (○), 1×10^{13} cm^{-2} (△), 2×10^{13} cm^{-2} (◇), and 5×10^{13} cm^{-2} (☆) and annealed at 680 °C for times ranging from 10 min to 15 h. At the lowest implantation dose shown in figure, the defect concentration is below the sensitivity limit of the DLTS system after 1 h annealing, as indicated by the arrow in figure. When the ion fluence is increased, up to 5×10^{13} cm^{-2}, the time necessary for cluster dissociation increases and a high defect concentration is present even after 15 h of annealing. This result shows that the I-clusters are more stable in temperature for higher implantation doses. Since a higher dose implies a higher I supersaturation, the results of Fig. 11 suggest that bigger clusters, more stable in temperature, are formed in this case.

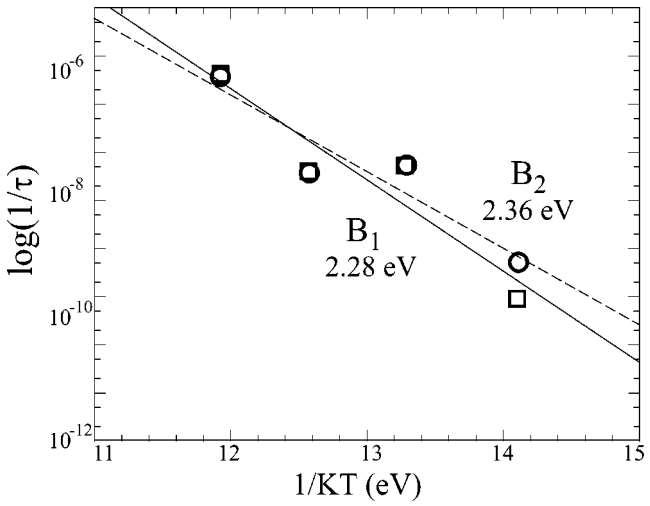

FIG. 10. Arrhenius plot of the B_1 (□) and B_2 (○) characteristic times. The solid and dashed lines are linear fits of the data.

C. Interstitial cluster characterization

In Sec. III B we pointed out that the optical spectra of I-clusters present broad features peculiarly different from the extremely sharp lines observed instead for point-like defects.

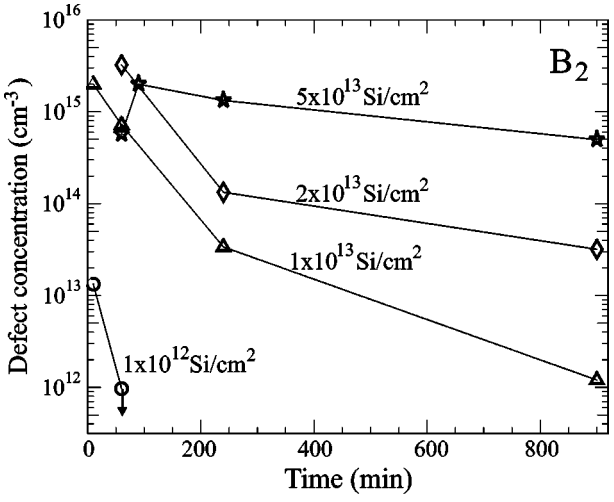

FIG. 11. Defect concentration values, as obtained from DLTS measurements, for p-type epitaxial Si samples implanted with 145 keV Si to doses of 1×10^{12} cm^{-2} (○), 1×10^{13} cm^{-2} (△), 2×10^{13} cm^{-2} (◇), and 5×10^{13} cm^{-2} (☆). The samples were annealed at 680 °C.

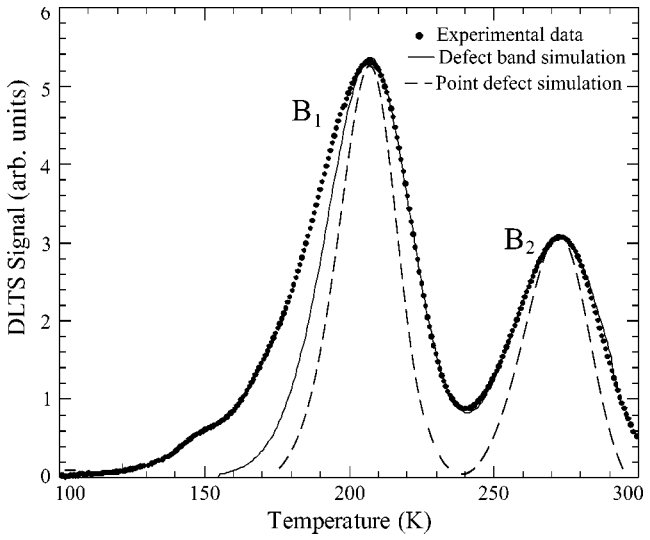

FIG. 12. DLTS spectrum (●) of a *p*-type Si sample implanted with 1.2 MeV Si to a dose of $1\times10^{12}\,\mathrm{cm}^{-2}$ and annealed at 700 °C for 20 min. The experimental data have been compared with the simulations obtained assuming that the defect signatures were introduced by point defects (dashed line) and defect bands (solid line).

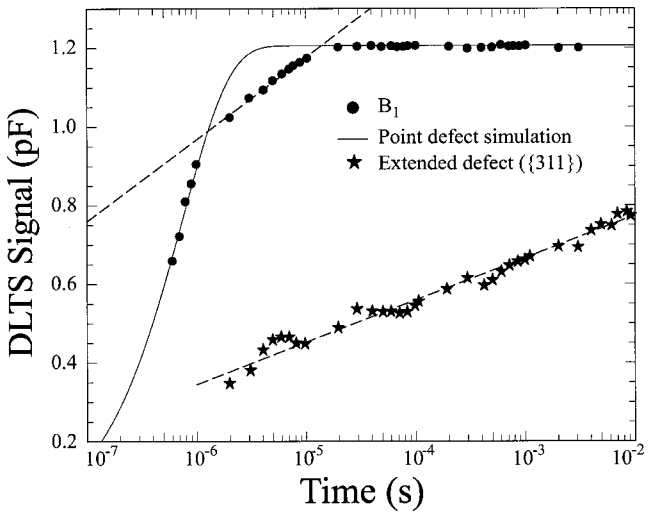

FIG. 13. Capture cross section measurements of B_1 (●) and {311} (★) electrical markers. The solid line is the expected capture cross section for a point-like defect. The two dashed lines are linear fit of the data. For the linear fit plotted for the B_1 capture cross section, only part of the points was used. The solid line is the point-like defect capture cross section.

Now we show that also the DLTS spectra of *I*-clusters exhibit much broader features than those expected for point-like defects. As an example, the DLTS spectrum of a *p*-type epitaxial Si sample implanted with 1.2 MeV Si to a dose of $1\times10^{12}\,\mathrm{cm}^{-2}$ and annealed at 700 °C for 20 min (●) has been compared, in Fig. 12, with the simulation of a DLTS spectrum (dashed line) of simple point-like defects. The simulation was performed assuming two point-like defects having the same activation energy and capture cross section experimentally determined for the *B*-line *I*-clusters. As evident from the figure, the point-defect simulation is much narrower than the experimental data, but they are in good agreement with the simulation curve (solid line) obtained with the procedure described later in the text. One of the possible causes of the observed broadening could be the convolution of signatures quite close in the DLTS spectrum. To minimize this effect, the annealing temperature of 700 °C and time for the sample shown in figure were chosen in order to have a good *B*-line signal in DLTS and to reduce as much as possible the contribution arising from other defect structures that are less stable in temperature.

Broadening of DLTS peaks may have different explanations. In order to rule out most of them, and to get more insight on the *I*-cluster nature, different measurements were performed. A peak broadening could result from the temperature dependence of the defect carrier capture kinetic, the ability of a defect to trap a carrier as a function of time. A simple point-like defect, such as C_iO_i, exhibits exponential capture kinetics since only one carrier can be trapped at each level. Therefore, the DLTS signal exponentially approaches a saturation value (when all traps are filled) as the pulse width increases. An example of exponential capture kinetics is shown as a solid line in Fig. 13, where the DLTS signal intensity as a function of the logarithm of the filling pulse duration is plotted. The carrier capture kinetics related to an extended defect exhibits fully logarithmic behavior, as plotted in figure. As an example, the capture kinetic of the {311} electrical marker is plotted as a straight line in graph in Fig. 13 (★). This last measurement was performed monitoring the {311} electrical signature at $E_v+0.50\,\mathrm{eV}$ observed in DLTS.[15] The straight line in figure is a guide to the eye and shows that the capture kinetic is fully logarithmic in this case. This behavior is a direct consequence of the extended nature of the defect, which is able to accommodate more than one carrier. The capture of a single carrier by the defect does not produce a net change in its charge state, since the carrier is ''delocalized'' either in defects ''surrounding'' the extended defect surface or in the extended defect core.[31] As a consequence of the charge storage at the defect, a Coulombic repulsion significantly reduces the rate at which other carriers are trapped on the same defect. The DLTS signal increases logarithmically with the pulse width and does not reach saturation.

Comparison of the capture cross section of the *I*-cluster signature (●) with that of point defects and the extended defects yields some hints about defect structure. The data refer to B_1 and are measured from an epi Si sample implanted with 1.2 MeV Si to a dose of $1\times10^{12}\,\mathrm{cm}^{-2}$ and annealed at 700 °C for 20 min. Similar behaviors have been detected for all the samples implanted with $1\times10^{12}\,\mathrm{Si/cm}^2$ annealed in the range 600–750 °C. The center exhibits a behavior that is a combination of exponential and logarithmic trends. For short filling pulses, until 1×10^{-7} s the measured trend can be well fitted by an exponential. An increase in the filling pulse duration results in a linear region well fitted by a straight line (dashed line in figure) and corresponding to a logarithmic capture kinetic. When the pulse duration is increased above $\geqslant10^{-5}$ s, the saturation in the DLTS signal is observed.

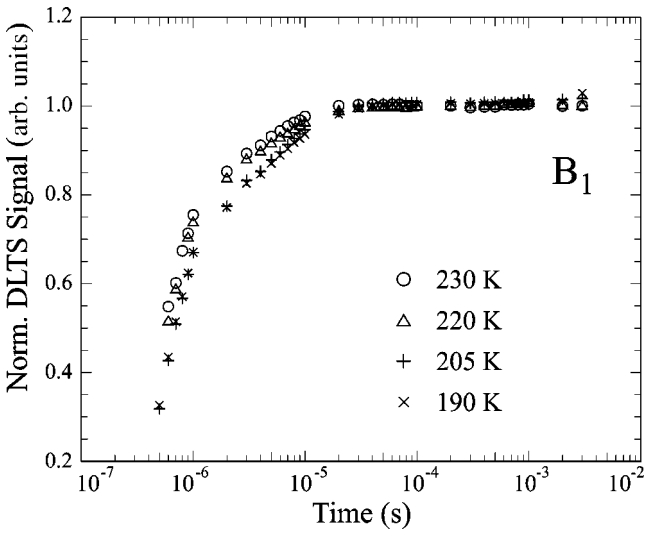

FIG. 14. Capture kinetics measurements of B_1 as a function of the sample temperature: 230 K (○), 220 K (△), 205 K (+), 190 K (×), for the *p*-type epitaxial Si sample implanted with 1.2 MeV Si to a dose of $1\times10^{12}\,\mathrm{cm}^{-2}$ and annealed at 600 °C for 30 min.

To rule out a temperature dependence of the capture cross section that could contribute to the observed peak broadening, capture kinetics measurements in the temperature range of 190–230 K were performed on both interstitial cluster signatures. The results are plotted in Fig. 14 for B_1 and are similar for B_2. The results do not show any temperature effect on the capture kinetics of the defects. The results could be explained by assuming that, since the cluster dimension is larger than that of a point defect, it can accommodate more than one carrier during the trapping process, as an extended defect does. However, since the clusters are smaller than an extended defect, there is an upper limit to the number of carriers that can be trapped by a single level, and the signal eventually saturates.

Another possible cause of peak broadening could be a field dependence of the trap emissivity.[32] However, measurements of the *B*-line signals show that the emissivities do not depend on the electric field, since Poole Frenkel effect was not detected on the two peaks as a function of the applied electric field. Any role of electric field variation was ruled out by performing the following experiment. Two different measurements were performed in an epi Si sample implanted with 1.2 MeV Si to a dose of $1\times10^{12}\,\mathrm{Si/cm}^2$ and annealed at 600 °C for 30 min. The reverse bias and filling pulse of 8 and 7.5 V, respectively, were used to monitor a region between 1.22 and 1.26 μm from the surface. In such a thin region there is only a small variation in the electric field. The results, plotted as a solid line in Fig. 15 for B_1 and being the same for B_2, show that the DLTS signatures exhibit the same broadening observed when sampling a larger region (dashed line). The two spectra have been normalized to allow direct comparison. A larger variation in the electric field is produced in this last case, since the reverse bias and filling pulse were 15 and 0.5 V, respectively. These results were confirmed in several other samples. In addition, as shown later in the paper, we have not detected any temperature effect on the capture kinetics of the defects: the measured

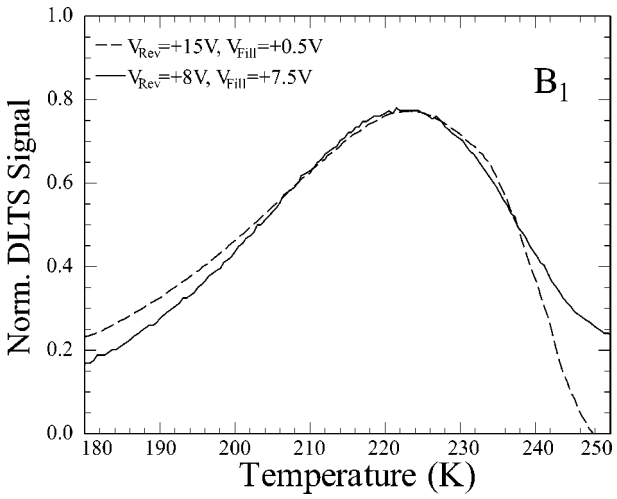

FIG. 15. DLTS measurements as a function of the electric field. The same broadening is observed when using 7.5–8 V (solid line) and 0.5–15 V as filling pulse and reverse bias, respectively. The broadening does not depend on the electric field distribution.

broadening cannot be associated with a temperature dependence of trap emissivity.

We believe that the broad DLTS signatures are related to a distribution of defect energy states in the Si band gap rather than to field or capture kinetic–related effects on a single level. The broadening could be associated with a spread in the emission energies from the deep levels. Examples reported in literature are highly dislocated[33,34] Si and the EL2 level[35] in $GaAs_{1-x}P_x$. Omling, Samuelson, and Grimmeis[33] have analyzed broad DLTS peaks and extracted the concentration and the energy spread of the deep levels. The analysis is based on the assumption that the deep levels in the gap that produce the broad peaks are not associated to a single level with activation energy E_0 but to a narrow band of levels that form a Gaussian distribution having E_0 as mean value and with a broadening described by an *S* factor. The DLTS signal[13,35] (ΔC) can be described as

$$C(t)=\int_0^\infty g(E)C_0\exp[-e_n^t(E)t]dE, \tag{2}$$

where C_0 is a normalizing factor and $g(E)$ is the broadening function given by[36]

$$g(E)=\frac{1}{\sqrt{2\pi}S}\exp[-(E-E_0)^2/2S^2]. \tag{3}$$

The data are fitted by varying the broadening factor *S*. Using this procedure, Ayres *et al.*[36] obtained an energy spread of ~35 meV for the DLTS signature of end-of-range extended defects in preamorphized crystalline Si.

An increase in the *S* factor both increases the width of the measured DLTS peaks and reduces the intensity of the signal. For this reason an equivalent defect concentration, N_S, is defined as the concentration that would be obtained from the DLTS measurements if the broadening factor *S* were zero. Moreover, it should be noted that the incorporation of a

defect complex, larger than a point-like defect, causes a large reconstruction of the lattice around it. As a result, the number of levels introduced in the gap by each complex can be much lower than the number of defects (i.e., interstitials) stored in it. This condition has been verified for extended defects[31,33,36] and it is reasonable to assume that it holds also for defect clusters. Therefore, the measured DLTS concentrations are correlated with the number of clusters rather than with the I stored in these clusters.

Finally, the data can be reproduced assuming a symmetric (Gaussian) broadening of the two energy levels. The results plotted as a solid line in Fig. 12 have been obtained analyzing the I-cluster DLTS signal using Eqs. (2) and (3). There is a good agreement between the simulation and the experimental data except at low temperatures, the difference arising from a contribution by an additional peak at ~150 K and/or to a nonperfectly Gaussian distribution of the defect states.[36] An S value of 19.5 and 17 meV was obtained for B_1 and B_2, respectively, for the sample plotted in Fig. 12. Since the measured peak heights are lowered as a consequence of the broadening, the fitting procedure also allowed us to extract the correct defect concentration N_S from the spectra.

It is interesting to note that the measured spectra are very similar, both in energy and temperature location to those determined by Ayres and Brotherton[36] for the DLTS signature of end-of-range extended defects in preamorphized crystalline Si, although the energy spread is much smaller, ~18 eV versus ~35 meV. This difference, observing that the B-lines are signatures of small interstitial clusters rather than those of extended defects, would suggest that the S parameter is sensitive to the dimension of the defect, increasing as the size increases, or to the stress around the defect.

The S variation with defect dimension has been characterized in the following experiment. p-type epitaxial Si samples were implanted with 145 keV or 1.2 MeV Si to a fluence of 1×10^{12}–$2\times10^{13}\,\mathrm{cm}^{-2}$ and annealed at temperatures ranging from 600 to 750 °C. The annealing temperature was chosen in order to minimize the broadening effects due to the convolution of more peaks. Changes in the thermal budget produced significant modifications in the DLTS peak broadening and defect concentrations. The same reverse bias and filling pulse were used for all measurements to eliminate any electric field effect dependence. The results for a sample implanted with 1.2 MeV Si to a fluence of $1\times10^{12}\,\mathrm{cm}^{-2}$ and annealed at 700 °C (★) are summarized in Fig. 16, where the S factor (left-hand scale) and the defect concentration N_S (right hand scale) for signatures B_1 [Fig. 16(a)] and B_2 [Fig. 16(b)] are plotted. Annealing for longer times resulted in a large increase of the S factor (up to ~25–28 meV) and a strong reduction in the total defect concentrations (N_S) by ~2 orders of magnitude. This behavior is similar for both B_1 and B_2.

The data so far reported clearly indicate that similar structures are found in regions having a variable local environment and/or a larger stress. The same structure can exhibit slightly different carrier emission energies either due to the lattice stress surrounding the defect, or as a consequence of the interaction between carriers trapped on clusters close to each other. Two possible explanations fit our data. Upon

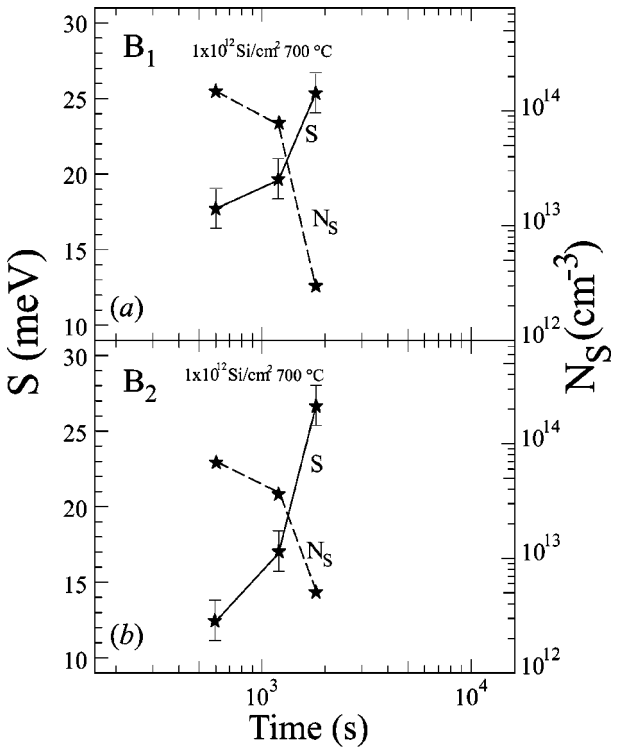

FIG. 16. Energy spread factor S (solid lines) and total defect concentration N_S (dashed lines) as a function of annealing time for (a) B_1 and (b) B_2. Data are plotted for p-type epitaxial Si samples implanted with 1.2 MeV Si, $1\times10^{12}\,\mathrm{cm}^{-2}$ and annealed at 700 °C (★).

annealing, clusters less stable in temperature dissociate releasing the interstitials they stored. An average decrease of the number of clusters (N_S) is expected. At the same time, the interstitials released by the dissolution of those clusters will join clusters more stable in temperature, increasing the stress around them and the associated S value. The other possible scenario is that, as the annealing proceeds, the small clusters that survive dissociation can coalesce and come closer to each other, as suggested by Monte Carlo simulation carried out by La Magna, Coffa, and Libertino.[37] The presence of a larger number of clusters in a smaller area produces a higher local stress. The S variation could be due either to a variation in the local stress around the defect or to the interaction of carriers trapped at different sites very close to each other. This S dependence from the stress and/or trapped carrier interactions would be the responsible for the high values reported for extended defects.[31]

Measurements on epitaxial Si samples implanted at 145-keV Si to a fluence of $2\times10^{13}\,\mathrm{cm}^{-2}$ and annealed at 680 °C for 4 h offer further insights into the physical meaning of the S values. The reduced range of 145-keV Si ions lie within the zero-bias depletion region, and only the tails of the damage distribution can be monitored by DLTS. In the inset of Fig. 17 the depth concentration profiles of B_1(■) and B_2 (★) are plotted and are compared to the extra implanted ion depth profile (solid line, divided by a factor of 100) simulated with MARLOWE. The comparison clearly shows that no long-range migration of interstitials is involved in the defect

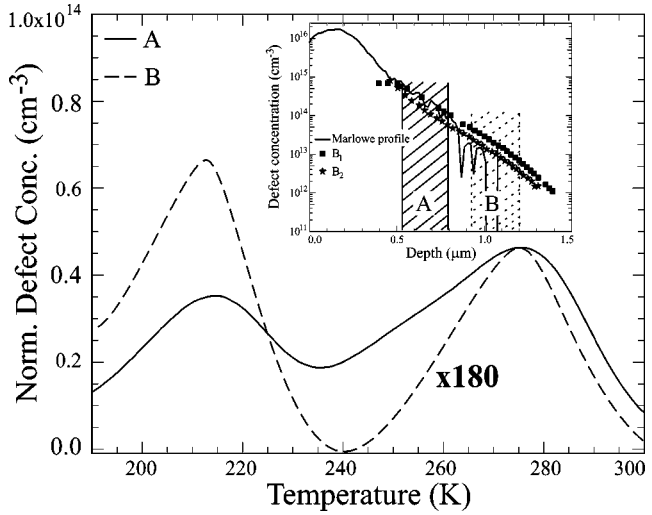

FIG. 17. DLTS analyses on a *p*-type epitaxial Si sample implanted with 145 keV Si to a dose of $2\times10^{13}\,\mathrm{cm}^{-2}$ and annealed at 680 °C for 4 h. Spectra were measured in region *A* (solid line, using $V_{\mathrm{Rev}}=+1$ V and $V_{\mathrm{Fill}}=0$ V) and region *B* (dashed line, using $V_{\mathrm{Rev}}=+7$ V and $V_{\mathrm{Fill}}=+4$ V). The last spectrum is multiplied by a factor of 900 in order to allow comparison. In the inset the depth-concentration profiles for B_1 (■) and B_2 (★) are plotted. The solid line is the simulation of the implanted-ion depth distribution according to MARLOWE.

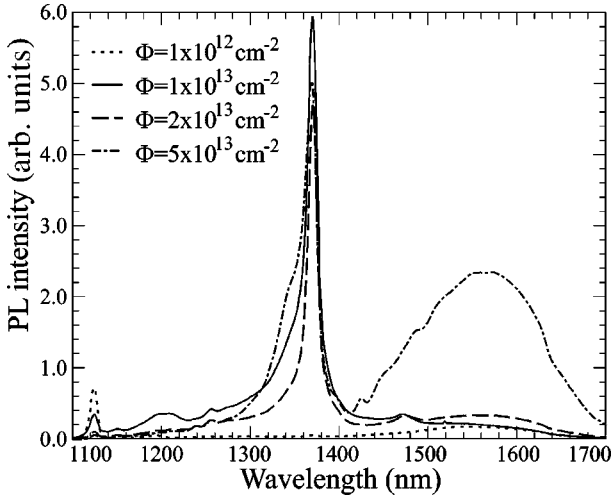

FIG. 18. PL spectra taken at 17 K on *n*-type Si samples implanted with 1.2 MeV Si to doses of $1\times10^{12}\,\mathrm{cm}^{-2}$ (dotted line), $1\times10^{13}\,\mathrm{cm}^{-2}$ (solid line), $2\times10^{13}\,\mathrm{cm}^{-2}$ (dashed line), and $5\times10^{13}\,\mathrm{cm}^{-2}$ (dash-dot-dashed line). The samples have been annealed at 680 °C for 1 h.

cluster formation, and regions of the sample at different depths experience different interstitial supersaturation. At the same time a larger stress and a closer spatial defect distribution are expected in the higher supersaturation region. If *S* is related to one of the two effects a different peak broadening in different regions is expected. DLTS measurements were performed in two different regions labeled as *A* (solid lines area in the inset) and *B* (dashed lines area in the inset). Region *A* was explored using a reverse bias $V_{\mathrm{rev}}=+1$ V and a filling pulse of $V_{\mathrm{fill}}=0$ V, while region *B* was explored using $V_{\mathrm{rev}}=+7$ V and $V_{\mathrm{fill}}=+4$ V. DLTS spectra recorded in the two regions are plotted in Fig. 17 as a solid and a dashed line for *A* and *B*, respectively. Once again, the same signatures B_1 and B_2 are present in both cases, but the DLTS spectrum of region *B* has been multiplied by a factor of 900 and subjected to a smoothing procedure to allow comparison. The calculated values for *S* are ~27 meV in region *A* and ~5 meV in region *B*. Since region *A* experienced a higher interstitial supersaturation during implantation than region *B*, both a larger stress and a denser cluster distribution are expected in this region. Thus the *S* dependence may result from both effects. The cluster density varies with depth due to the interstitial supersaturation distribution during implant; hence both the stress of the lattice around the defects and the defect dimensions are larger in the region that experienced the highest *I* supersaturation.

On the basis of these results, the *S* data plotted in Fig. 16 should be regarded as an average of the cluster distribution or of the stress distribution. However, the contribution of the clusters present in the tail of the ion distribution is expected to be very small due to their low concentration (see Fig. 17). In addition, their contribution will decrease at longer annealing times.

D. Extended defect formation

Si ion implantation to doses $\geqslant5\times10^{13}\,\mathrm{Si/cm}^2$ and annealing temperatures ⩾680 °C for 1 h is known to cause the formation of extended defects, in particular {311} rod-like defects,[12] which have been widely characterized by TEM analysis. Recently we have shown[15,20] that {311} defects exhibit an electrical signature in Si visible by DLTS, as mentioned in the previous section. Such a signature has been identified as the electrical marker of the {311} defects monitoring by TEM the {311} evolution and by DLTS the signature evolution as a function of the annealing conditions on the same samples. In this work, we used DLTS and PL measurements to characterize extended defects and to observe the transition from *I*-clusters to extended defects. When the annealing temperature is increased to 680 °C a new regime is entered, characterized by major modifications in the optical and structural properties of *I*-type defects. The PL spectra for the samples implanted with 1.2 MeV Si at doses in the range 1×10^{12}–$5\times10^{13}\,\mathrm{cm}^{-2}$ and annealed at 680 °C for 1 h are plotted in Fig. 18. At the lowest dose ($1\times10^{12}\,\mathrm{Si/cm}^2$, dotted line) the damage is fully recovered and the spectrum only reveals the 1121 nm signature due to Si band-edge phonon-assisted recombination.[18] However, at doses $\geqslant10^{13}\,\mathrm{cm}^{-2}$ in samples with a low C concentration ($\sim10^{16}\,\mathrm{cm}^{-3}$) a sharp peak at 1376 nm (0.9007 eV) dominates the spectra. The width of this peak slightly increases with the ion-implantation dose and a broad band centered at 1550 nm is developed at the highest dose ($5\times10^{13}\,\mathrm{cm}^{-2}$). We performed a TEM analysis on all of the samples and those implanted at doses $\geqslant1\times10^{13}\,\mathrm{cm}^{-2}$ revealed the presence of {311} planar defects.[21] A one-to-one correlation exists between the observation of the PL line at 1376 and the presence of a large concentration of {311} defects in the sample, and this line has been associated to optical transition occurring at or close to {311} defects.[21] This result points to the PL as a promising technique to fully characterize the extended

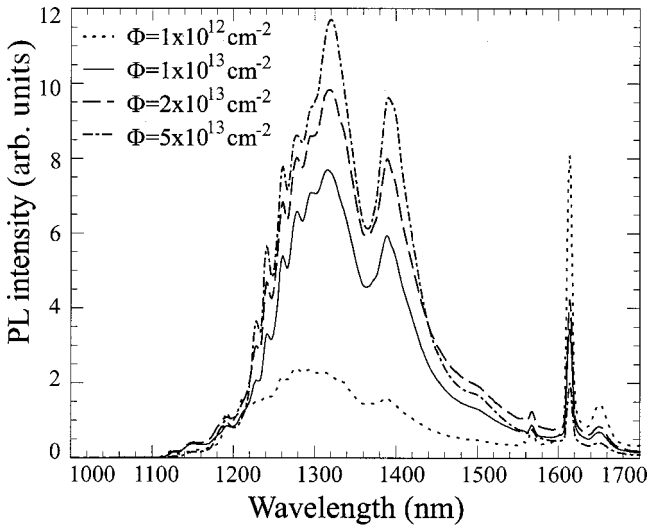

FIG. 19. PL spectra taken at 17 K on *n*-type Si samples implanted with 1.2 MeV Si to doses of $10^{12}\,\mathrm{cm}^{-2}$ (dotted line), $1\times10^{13}\,\mathrm{cm}^{-2}$ (solid line), $2\times10^{13}\,\mathrm{cm}^{-2}$ (dashed line), and $5\times10^{13}\,\mathrm{cm}^{-2}$ (dash-dot-dashed line). The samples were annealed at 600 °C for 15 h.

defect formation. In fact, the presence of {311} defects in DLTS is determined by a level at $E_V+0.50$ eV in a spectrum in which are still present the *I*-cluster electrical markers that lie very close to the {311} peak in the spectrum. When extended defects form the optical properties of the sample are totally modified and their presence is clearly visible by the presence of the 1376 nm line.

The results shown in Fig. 18 clearly indicate the presence of a threshold dose for the formation of extended {311} defects. Previous measurements[26] we performed on CZ Si with a carbon content $\geqslant5\times10^{16}\,\mathrm{cm}^{-3}$ showed a threshold dose for extended defect formation $>2\times10^{13}\,\mathrm{Si/cm}^2$. In the Czochralski-grown Si with a low carbon content ($\sim10^{16}\,\mathrm{cm}^{-3}$) we used in this work, the threshold is much lower, certainly lower than $1\times10^{13}\,\mathrm{cm}^{-2}$. The formation of {311} extended defects at relatively low dose, $1\times10^{13}\,\mathrm{Si/cm}^2$, in these samples is in agreement with the literature data, confirming the presence of a lower threshold dose in highly pure materials. In fact, it is known[7] that the threshold dose for {311} defect formation is reduced when the impurity concentration is lower. As previously mentioned, this has been attributed to the fact that C stores interstitials, thus preventing the formation of big self-interstitial clusters and, eventually, extended defects. If the C concentration in the sample is strongly reduced, the threshold dose for {311} formation is expected to change.

We characterized the extended defect formation as a function of the annealing temperature and time. To this purpose samples implanted with 1.2-MeV Si to doses of $1\times10^{12}\,\mathrm{cm}^{-2}$ (dotted line), $1\times10^{13}\,\mathrm{cm}^{-2}$ (solid line), $2\times10^{13}\,\mathrm{cm}^{-2}$ (dashed line), and $5\times10^{13}\,\mathrm{cm}^{-2}$ (dot-dashed line) were annealed at 600 °C for times up to 15 h. The PL spectra of the residual damage for these samples are compared in Fig. 19. If the presence of *I*-cluster optical signatures for the sample implanted at the lowest dose is perfectly understandable, the same is not true for the other samples. In fact, even at the highest implantation dose ($5\times10^{13}\,\mathrm{Si/cm}^2$) only the *I*-cluster signatures are present in the spectrum. This result has been confirmed by our high-resolution PL spectra and TEM analysis. These last measurements only reveal the presence of a region with a high strain centered at $\sim1.35\ \mu$m from the surface, at the end-of-range of 1.2 MeV Si.[21]

Finally, PL measurements performed on samples annealed at 600 °C for times of 30 h do not show the presence of {311} defects, thus confirming the presence of a threshold temperature. These result are in perfect agreement with the Monte Carlo simulations on lattice recently carried out by La Magna, Coffa, and Libertino. They showed that the *I*-cluster evolution into extended defects cannot occur through a simple Ostwald ripening mechanism. In fact, the *I*-cluster structures most stable for small aggregates, derived by tight-binding calculations,[11] are different from the {311} structure. A structural transformation of the *I*-clusters has to occur before they can grow into extended defects. Only after this transformation occurs the ''traditional'' OR takes place and the extended defect regime is entered. Our results fit also with the explanation proposed by Cowern *et al.*[9] In fact, they assume a very stable *I*-cluster configuration (with about eight interstitials) and a large potential barrier before the OR can take place. We believe that the ''magic number'' they find arises from the fact that at a certain size the clusters must undergo a structural transformation in order to grow larger.

IV. CONCLUSIONS

This work reviews the main results we found on interstitial cluster formation, dissociation, and evolution into extended {311} defects. After low-dose implantation, $10^9-10^{11}\,\mathrm{Si/cm}^2$, second-order point defects, interstitial related, form. They dissociate at temperatures $\leqslant550$ °C. Intermediate-dose implantation, $10^{12}-10^{13}\,\mathrm{Si/cm}^2$, and annealing at temperatures in the range 550–700 °C produces interstitial clusters. We widely characterized their properties and found the following.

(1) *I*-clusters introduce both electrical signatures with activation energies of $E_v+0.33$ eV and $E_v+0.52$ eV and optical signatures centered at 1320 nm (0.94 eV) and 1390 nm (0.89 eV).

(2) C, O, or dopants influence the clustering process, probably acting either as preferential nucleation centers for small *I*-clusters or by trapping interstitials and preventing them from annihilation at the surface.

(3) *I*-clusters are present in a dose and temperature regime at which B TED occurs without the formation of extended defects. Their dissociation energy varies as a function of the implantation dose, but the measured dissociation energy value for *I*-clusters at $1\times10^{12}\,\mathrm{Si/cm}^2$, ~2.3 eV, is in good agreement with those observed for low-fluence TED.

(4) Broadening of both the electrical and optical *I*-cluster signatures have been observed. It is more pronounced in regions that experience a higher *I* supersaturation and increases as a function of the annealing time. The data clearly indicate that similar structures are found in regions having a variable local environment and/or a larger stress.

High-dose implantation, $\geqslant 10^{13}$ Si/cm^2, and annealing at temperatures above 680 °C causes the {311} extended defect formation. The {311} defect presence is detectable by both electrical (with a signature at $E_v + 0.50$ eV) and optical (with a PL signal at 1376 nm) measurements. PL measurements allowed us to follow the transition from *I*-clusters to extended defects and to find that a threshold dose ($>1 \times 10^{12}$ cm^{-2}), determined by the impurity content of the material, and a threshold temperature (>600 °C) exists for {311} extended defect formation.

All the results reported in this paper strongly indicate that a well-defined structural transition occurs in the evolution from *I*-clusters to extended defects. These result suggest that the defect agglomeration does not undergo a simple Ostwald ripening mechanism at every size.

ACKNOWLEDGMENTS

The authors acknowledge Aldo Spada and Nicolò Parasole for the invaluable technical assistance and Dale C. Jacobson and Antonio Marino for the implants. The work in Catania was partially supported by Progetto 5% Microelettronica and Progetto Finalizzato MADESS II.

[1] K. S. Jones, J. Liu, L. Zhang, V. Krishnamoorthy, and R. T. DeHoff, Nucl. Instrum. Methods Phys. Res. B **106**, 227 (1995).
[2] A. E. Michel, W. Rausch, P. A. Ronsheim, R. H. Kastl, Appl. Phys. Lett. **50**, 416 (1987).
[3] M. Giles, J. Electrochem. Soc. **138**, 1160 (1991).
[4] P. A. Stolk, H.-J. Gossmann, D. J. Eaglesham, D. C. Jacobson, C. S. Rafferty, G. H. Gilmer, M. Jaraiz, J. M. Poate, H. S. Luftman, and T. E. Haynes, J. Appl. Phys. **81**, 6031 (1997).
[5] D. J. Eaglesham, P. A. Stolk, H.-J. Gossmann, J. M. Poate, Appl. Phys. Lett. **65**, 2305 (1994).
[6] L. H. Zhang, K. S. Jones, P. H. Chi, and D. S. Simons, Appl. Phys. Lett. **67**, 2025 (1995).
[7] H. G. Huizing, Ph.D. dissertation, University of Delft, The Netherlands, 1996.
[8] P. B. Hirsch, A. Howie, R. B. Nicholson, D. W. Pashley, and M. J. Whelan, *Electron Microscopy of Thin Crystals* (Butterworths, London, 1965).
[9] N. E. B. Cowern, G. Mannino, P. A. Stolk, F. Rooseboom, H. G. A. Huizing, J. G. M. van Berkum, F. Cristiano, A. Claverie, and M. Jaraiz, Phys. Rev. Lett. **82**, 4460 (1999).
[10] P. W. Voorhees and M. E. Glicksman, Acta Metall. **32**, 2001 (1984).
[11] A. Bongiorno, L. Colombo, F. Cargnoni, C. Gatti, and M. Rosati, in *Proceedings of the 24th International Conference on the Physics of Semiconductors*, edited by D. Gershoni (World Scientific, Singapore, 1999).
[12] T. Y. Tan, Philos. Mag. **44**, 101 (1981).
[13] D. V. Lang, J. Appl. Phys. **45**, 3023 (1974); **45**, 3014 (1974).
[14] S. Libertino, J. L. Benton, D. C. Jacobson, D. J. Eaglesham, D. J. Eaglesham, J. M. Poate, S. Coffa, P. Kringhoj, P. G. Fuochi, and M. Lavalle, Appl. Phys. Lett. **71**, 389 (1997).
[15] J. L. Benton, S. Libertino, P. Kringhoj, D. J. Eaglesham, J. M. Poate, and S. Coffa, J. Appl. Phys. **82**, 120 (1997).
[16] J. L. Benton, S. Libertino, D. J. Eaglesham, and S. Coffa, in *Defects and Diffusion in Silicon Processing*, edited by T. Diaz dela Rubia, S. Coffa, P. A. Stolk, and C. S. Rafferty, MRS Symposia Proceedings No. 469 (Materials Research Society, Pittsburgh, 1997), p. 193.
[17] J. L. Benton, K. Halliburton, S. Libertino, D. J. Eaglesham, and S. Coffa, J. Appl. Phys. **84**, 4749 (1998).
[18] G. Davies, Phys. Rep. **176**, 83 (1989).
[19] M. Nakamura, S. Nagai, Y. Aokiand, and H. Naramoto, Appl. Phys. Lett. **72**, 1347 (1998).
[20] S. Libertino, J. L. Benton, S. Coffa, and D. J. Eaglesham, in *Atomistic Mechanisms in Beam Synthesis and Irradiation of Materials*, edited by J. C. Barbour, S. Roorda, and D. Ila, MRS Symposia Proceedings No. 504 (Materials Research Society, Warrendale, PA, 1998), p. 3.
[21] S. Coffa, S. Libertino, C. Spinella, Appl. Phys. Lett. **76**, 321 (2000).
[22] H. Weman, B. Monemar, G. S. Oehrlein, and S. J. Jeng, Phys. Rev. B **42**, 3109 (2000).
[23] N. S. Minaev and A. V. Mudryi, Phys. Status Solidi **68**, 561 (1981).
[24] M. T. Robinson and J. M. Torrens, Phys. Rev. B **9**, 5008 (1974).
[25] S. Nishikawa, A. Tanaka, and T. Yamajl, Appl. Phys. Lett. **60**, 2270 (1992).
[26] P. A. Stolk, H.-J. Gossmann, D. J. Eaglesham, D. C. Jacobson, and H. S. Luftman, in *Beam-Solid Interactions for Materials Synthesis and Characterization*, edited by D. E. Luzzi, T. F. Heinz, M. Iwaki, and D. C. Jacobson, MRS Symposia Proceedings No. 354 (Materials Research Society, Pittsburgh, 1995).
[27] H.-J. Grossman, C. S. Rafferty, H. S. Luftman, F. C. Unterwald, T. Boone, and J. M. Poate, Appl. Phys. Lett. **63**, 639 (1993).
[28] L. W. Song and G. D. Watkins, Phys. Rev. B **42**, 5759 (1990).
[29] G. Davies, K. T. Kun, and T. Reade, Phys. Rev. B **44**, 12 146 (1991).
[30] S. Libertino, S. Coffa, C. Spinella, J. L. Benton, and D. Arcifa, Mater. Sci. Eng. B **71**, 137 (2000).
[31] V. V. Kveder, Yu. A. Osipyan, W. Schroeter, and G. Zoth, Phys. Status Solidi A **72**, 701 (1982).
[32] P. Blood and J. W. Orton, in *The Electrical Characterization of Semiconductors: Majority Carriers and Electron States*, edited by N. H. March (Academic, London, 1992).
[33] P. Omling, L. Samuelson, H. G. Grimmeiss, J. Appl. Phys. **54**, 5117 (1983).
[34] L. Samuelson and P. Omling, Phys. Rev. B **34**, 5603 (1986).
[35] P. Omling, E. R. Weber, L. Montelius, H. Alexander, and J. Michel, Phys. Rev. B **32**, 6571 (1985).
[36] J. R. Ayres and S. D. Brotherton, J. Appl. Phys. **71**, 2702 (1992).
[37] A. La Magna, S. Coffa, and S. Libertino, in *Si Front-End Processing: Physics and Technology of Dopant-Defect Interactions II*, edited by A. Agarwal and L. Pelaz, MRS Symposia Proceeding No. 610 (Materials Research Society, Warrendale, PA, 2000).